AIP | APL Materials

Structurally stabilized mesoporous TiO2 nanofibres for efficient dye-sensitized solar cells

Fargol Hasani Bijarbooneh, Yue Zhao, Ziqi Sun, Yoon-Uk Heo, Victor Malgras, Jung Ho Kim, and Shi Xue Dou

Citation: APL Mater. **1**, 032106 (2013); doi: 10.1063/1.4820425
View online: http://dx.doi.org/10.1063/1.4820425
View Table of Contents: http://scitation.aip.org/content/aip/journal/aplmater/1/3?ver=pdfcov
Published by the AIP Publishing

Structurally stabilized mesoporous TiO_2 nanofibres for efficient dye-sensitized solar cells

Fargol Hasani Bijarbooneh,[1] Yue Zhao,[1,2] Ziqi Sun,[1] Yoon-Uk Heo,[3] Victor Malgras,[1] Jung Ho Kim,[1,a] and Shi Xue Dou[1]

[1]*Institute for Superconducting and Electronic Materials, University of Wollongong, Squires Way, North Wollongong, New South Wales 2500, Australia*

[2]*School of Mechanical, Materials and Mechatronic Engineering, University of Wollongong, Northfields Ave, Wollongong, New South Wales 2522, Australia*

[3]*Research Facility Center, Graduate Institute for Ferrous Technology, Pohang University of Science and Technology, Pohang, Kyungbuk 790-784, South Korea*

(Received 10 May 2013; accepted 12 July 2013; published online 6 September 2013)

One-dimensional (1D) TiO_2 nanostructures are very desirable for providing fascinating properties and features, such as high electron mobility, quantum confinement effects, and high specific surface area. Herein, 1D mesoporous TiO_2 nanofibres were prepared using the electrospinning method to verify their potential for use as the photoelectrode of dye-sensitized solar cells (DSSCs). The 1D mesoporous nanofibres, 300 nm in diameter and 10-20 μm in length, were aggregated from anatase nanoparticles 20-30 nm in size. The employment of these novel 1D mesoporous nanofibres significantly improved dye loading and light scattering of the DSSC photoanode, and resulted in conversion cell efficiency of 8.14%, corresponding to an ~35% enhancement over the Degussa P25 reference photoanode. [http://dx.doi.org/10.1063/1.4820425]

Titanium dioxide (TiO_2) has been widely studied for photovoltaic cells because of its wide band gap (3.0-3.2 eV), cost-effectiveness, and environmental friendliness.[1–3] In particular, the tailored morphology of TiO_2 nanostructures undoubtedly plays a key role in determining their electrical conductivity and cell efficiency.[4,5] For example, one-dimensional (1D) TiO_2 nanostructures have shown unique properties in electronic and photonic devices from the viewpoint of charge transport.[6–10] The charge transport in the photovoltaic cell is always associated with diffusion, and it is strongly limited by the trapping and de-trapping between particles.[11–14] The slow electron transport between TiO_2 particles normally increases the rate of recombination of carriers with electrolyte.[15–18]

Recently, vertically structured TiO_2 nanoarrays, which were grown in a perpendicular direction to the working electrode, have shown the best performance due to the reduced trapping of photoinjected electrons along their path to the electrode[18–21] in dye-sensitized solar cells (DSSCs). A maximum power conversion efficiency of 6.9% was achieved with TiO_2 nanotubes prepared by anodization of Ti sheet.[22] This process is highly complicated, however, due to the complex synthesis process, and therefore, it needs to be simplified. In addition, this process is neither suitable for mass production, nor is the nanotube form stabilized under the heat-treatment process, i.e., nanowires are preferentially produced rather than nanotubes. Moreover, the low surface area and inferior dye adsorption of the single-crystalline TiO_2 1D nanostructures (nanorods and nanowires) have prevented high efficiencies from being achieved. For further improvement of the performance of DSSCs, 1D TiO_2 nanostructures need to be developed that combine the merits of both fast electron pathways and high surface area for sufficient dye adsorption.

[a]Author to whom correspondence should be addressed. Electronic mail: jhk@uow.edu.au

If optimization of favourable architectures is achieved through a simple method, highly stabilized 1D TiO_2 nanostructures can possess high surface area to absorb more dye and also enhance light harvesting efficiency by scattering more light in the red part of the solar spectrum.[23–25] In order to achieve this, 1D structured TiO_2 nanofibres with high surface area were prepared by using electrospinning. Electrospinning is known to be a simple and versatile method for obtaining fibre structures which are long in length and uniform in diameter.[26–28] In this study, therefore, these nanofibres were directly adopted as high-performance photoelectrode for dye-sensitized solar cells.

TiO_2 nanofibers were prepared from a sol-solution of 1.5 ml titanium isopropoxide (97%, Sigma Aldrich), 3 ml acetic acid (99.7%, Sigma Aldrich), and 3 ml ethanol (99.8%, Sigma Aldrich). Then, an ethanolic solution of 0.45 g polyvinylpyrrolidone (PVP, MW = 1 300 000, Sigma Aldrich) and 3.5 ml ethanol (Sigma Aldrich) was added to the prepared TiO_2 sol-solution. This solution was immediately loaded into a plastic syringe equipped with a needle for electrospinning. The applied voltage, discharge distance, and injection rate were 17 kV, 12 cm, and 0.8 ml h^{-1}, respectively. The obtained TiO_2 nanofibres were then calcined at an optimized temperature of 650 °C for 3 h. In order to decrease the limiting factors due to a lower recombination rate, the blocking layer technique was also adopted for some of the DSSCs. To construct the DSSCs, fluorine doped tin oxide (FTO, SnO_2:F, 7 Ω sq^{-1}, Pilkington TEC Glass™) glass was dip-coated in the same TiO_2 sol-solution, if one was used. Then, the doctor blade technique was subsequently used to deposit the nanofibres (approximately 100 μm in thickness) on the FTO coated glass. The annealed TiO_2 photoanodes (approximately 10 μm in thickness) were immersed in 0.5 mM ruthenium dye (N719, Sigma Aldrich) dissolved in an acetonitrile (Sigma Aldrich), tert-butanol (Sigma Aldrich), and ethanol (1:1:2 ml) solvent mixture and held for 24 h in a dark place. The electrode was then rinsed in acetone to remove the excess dye and dried at room temperature. A platinum coated FTO glass slide for the counter electrode was clipped with the dye adsorbed TiO_2 electrode (working electrode) to make the cell. The space between the electrodes was filled with Iodolyte AN-50 electrolyte (iodide based low viscosity electrolyte with 50 mM of triiodide in acetonitrile) purchased from Solaronix. The final active region was 0.16 cm^2 for all the cells.

The phase structure was estimated by X-ray diffraction (XRD, GBC Scientific Equipment, Hampshire, Illinois, USA) using Cu$K\alpha$ radiation. High magnification images of the microstructure were obtained using a transmission electron microscope (TEM, JEOL JEM-2100F, Tokyo, Japan). The dye loading is measured by desorption of dye from TiO2 electrode into 0.1 M NaOH solution (water/ethanol = 1:1, v/v). Then the absorbance of the dye solution is measured by ultraviolet-visible (UV-Vis) absorption. The photocurrent density-voltage (J-V) characteristics were measured by exposing the cells to air mass (AM) 1.5 simulated sunlight from a solar simulator (PEL-L12, Peccell Technologies, Yokohama, Japan) in combination with a Keithley 2400 (Keithley Instrument, Cleveland, OH, USA) source meter. The incident photon-to-current quantum conversion efficiency (IPCE) was measured as an action spectrum, which uses an optical fiber (3 mm in diameter) for monochromatic irradiation (PEC-S20DC, Peccell Technologies, Yokohama, Japan). The monochromatic photocurrent was monitored by the continuous irradiation (dc measurement) method.

To obtain the optimized heating temperature for our TiO_2 nanofibre heat treatment, the phase composition of the nanostructure was examined for samples sintered within the temperature range of 500 °C–800 °C. Figure 1 shows the variation of rutile content, the full width at half maximum (FWHM) values of the anatase (101) peak, and the grain size of the nanofibres as a function of heating temperature, based on the XRD patterns. Here, the grain size was estimated from the FWHM of the anatase (101) peak by using the Scherrer formula (Figure 1(a)). It has been reported that anatase phase tends to transform to rutile phase above 550 °C.[29,30] Interesting enough, our nanofibres were quite stable, as can be seen in Figure 1(b). That is, only anatase phase existed, without any other phases, even up to 650 °C. It is well known that the thermodynamic properties of TiO_2 nanostructured materials have a strong relationship to the surface area or grain size.[31,32] The crystalline/grain size of our nanofibres, as shown in Fig. 1(c), was smaller than 30 nm after calcination. Therefore, due to the small grain size and thus the high surface energy, the nanofibres show a dominant anatase phase, even when calcined at 650 °C. The FWHM values of the anatase (101) peak become narrower with increasing sintering temperature (Figure 1(b)). This behaviour of the nanofibres as a function of sintering temperature can be explained by the improvement of

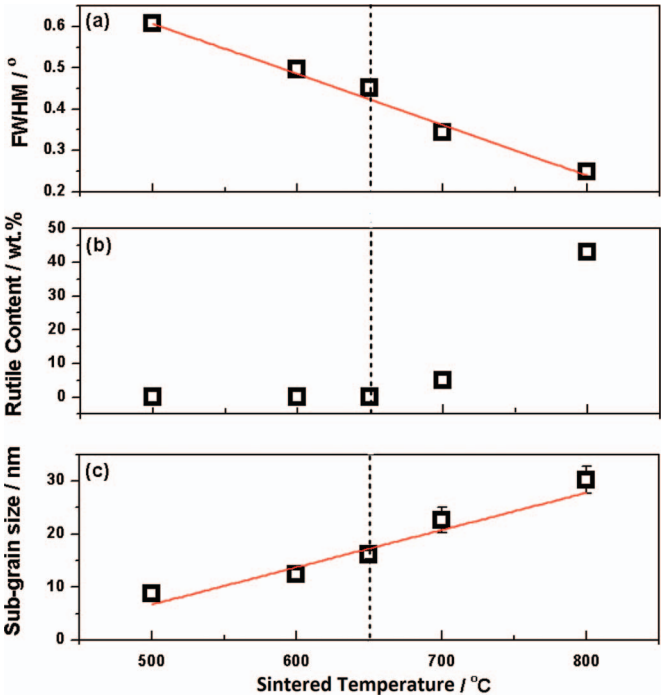

FIG. 1. (a) FWHM of the anatase (101) peak, (b) rutile content, and (c) sub-grain size as a function of sintering temperature.

crystallinity, resulting in increasing crystalline size (Figure 1(c)). Improvement of crystallinity is also associated with the connectivity between TiO_2 particles because nanosized TiO_2 nanoparticles are aggregated to form TiO_2 nanofibres. Based on our experimental conditions, therefore, TiO_2 nanofibres prepared by the electrospinning process were sintered at 650 °C for 3 h for testing in DSSCs.

For a better understanding of the microstructure of the electrospun nanofibres, the configuration and crystalline structure of the as-prepared TiO_2 nanofibres were observed using TEM. Figure 2 presents TEM images of the TiO_2 nanofibres from low to high magnification. Based on a statistical analysis of the nanofibres, as can be seen in Figures 2(a) and 2(b), the diameter and length of the TiO_2 fibres were estimated to be 300 nm and 10-20 μm, respectively. It has to be noted that there is mesoporous structure in the 1D nanofibres, which would be greatly helpful in enhancing the chemically active surface area (Figures 2(c) and 2(d)). Using the Brunauer-Emmett-Teller (BET) method, the specific surface area of the sintered nanofibres was determined to be 86 $m^2\,g^{-1}$, which is higher than the 50 $m^2\,g^{-1}$ of commercial P25 TiO_2 nanopowders. In the application of these 1D nanofibres in DSSCs, the high specific surface area can absorb more dye, which will lead to superior power cell efficiency. From the viewpoint of electron transport, the interface between TiO_2 particles is crucial because it has a decisive influence on the electron mobility. For this purpose, 1D structures, i.e., the nanowire/nanofibre/nanotube structures, are preferred over the 0D structure, i.e., nanoparticles. In addition, fibres prepared by the electrospinning method consist of well-crystallized and randomly distributed single phase, as shown in Figure 2(e). The selected area electron diffraction (SAED) pattern in Figure 2(f) clearly confirms that there are no other phases apart from anatase. The grain size calculated from Fig. 2(e), around 10 nm, was also confirmed by the small crystallites in the nanofibres.

Figure 3 shows the UV-Vis spectra of the mesoporous 1D TiO_2 nanofibres together with reference Degussa P25 nanoparticles. The absorbance onset of the nanofibres was around 400 nm, and the corresponding band gap was around 3.14 eV, which shows an obvious red-shift compared with the P25 nanoparticles. The latter presented an onset absorbance of 370 nm, and a band gap of 3.22 eV. Based on the previous reports[33,34] on shifts in the band gap, a smaller particle size will result in

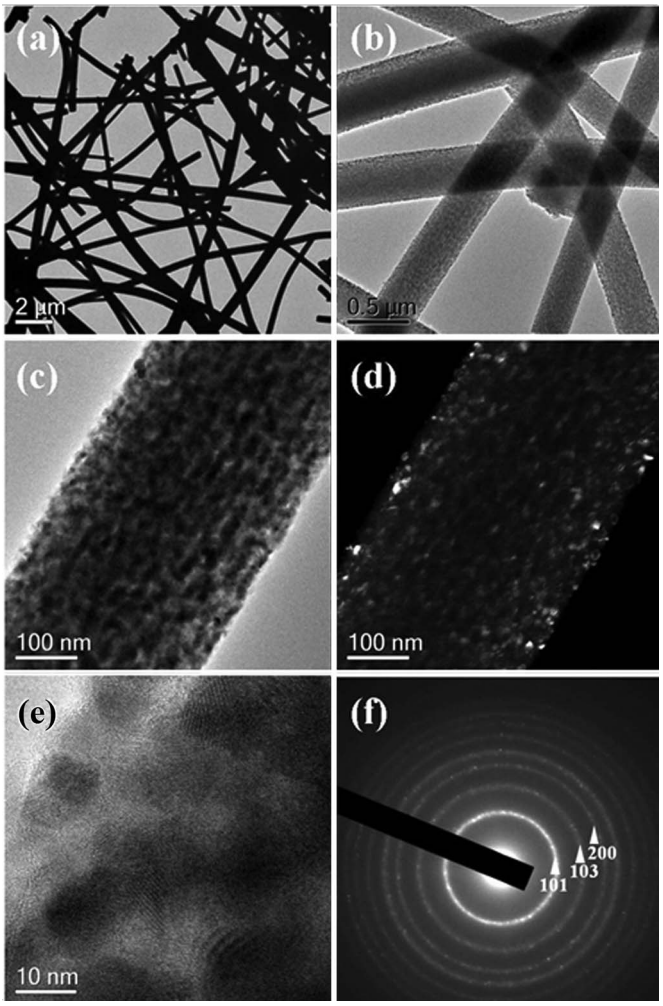

FIG. 2. TEM images of the TiO_2 nanofibre: (a)–(c) bright field images at different magnification, (d) dark field image, (e) high resolution image, and (f) SAED pattern.

a wider band gap. In this study, however, a narrow band gap was observed, even though the sub grain size was found to be on the order of 10 nm. Actually, when we carefully checked the UV-Vis spectrum of the nanofibres in the wavelength range of 320-360 nm, the curve was not as smooth as the one for P25, which is due to the nanoscale range of the particle sizes. The dye loading is measured to confirm the nanocrystalline structure of the nanofibres (Table I). As expected, the dye loading of the nanofibre samples is higher than the P25 samples, which corresponds to the higher surface area and nanosized particle. At the same time, owing to the scattering effect of the large sizes of the diameter and length of the fibres, which are around 300 nm and 10-20 μm, respectively, the UV-Vis spectrum would be expected to show enhanced light absorption in the visible light range. As a summation of these two contrary effects, the absorbance onset for the nanofibres shows a red shift. However, it should be noted that this red shift is due to light scattering, not band gap narrowing. The visible light scattering undoubtedly will increase the light absorbance in the photoanode and thus enhance the device performance.

Figure 4(a) shows the photocurrent density-voltage (J-V) curves of the cells prepared with an anatase TiO_2 nanofibre layer (NF-1) with a thickness of 10 μm. For a comparative study, we also prepared a reference cell (P25-1) with a commercial P25 thin film with the same thickness. These cells were not constructed with a blocking layer. The summarized results on short-circuit current density (J_{sc}), open-circuit voltage (V_{oc}), fill factor (FF), and power conversion efficiency (η) are

TABLE I. Solar efficiency (η), open circuit voltage (V_{oc}), short circuit current (J_{sc}), and fill factor (FF) of the prepared samples.

Samples I.D.	P25-1	P25-2	NF-1	NF-2
η [%]	5.16	6.03	7.28	8.14
V_{oc} [V]	0.74	0.73	0.76	0.76
J_{sc} [mA cm^{-2}]	9.80	11.28	13.69	15.23
Fill factor (FF)	0.70	0.72	0.70	0.70
Dye absorption [μmol cm^{-2}]	0.088	0.097	0.110	0.116

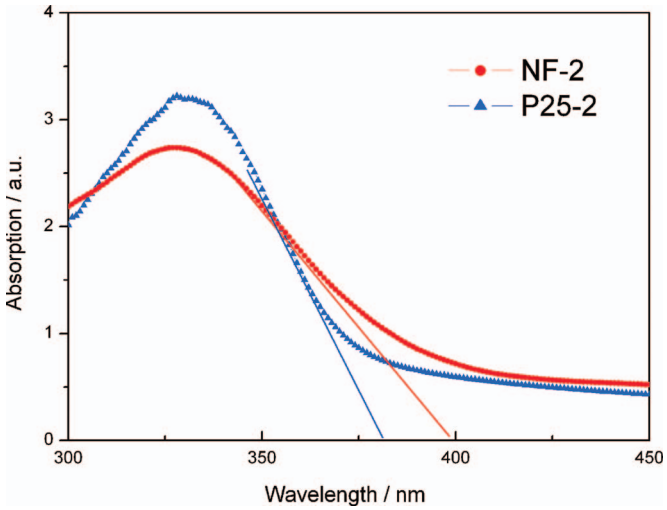

FIG. 3. UV-Vis spectra of nanofibers and P25 nanopowders.

presented in Table I. The V_{oc} values were very similar between the two samples: 0.74 V for P25-1 and 0.76 V for NF-1. By contrast, the J_{sc} of the cell prepared with the TiO_2 nanofiber photoanode was noticeably increased which is due to the increased dye loading from 0.088 μmol cm^{-2} to 0.097 μmol cm^{-2}. The improvement in the J_{sc} in turn resulted in a dramatic enhancement in cell efficiency. Compared to the reference P25 cell, which showed an efficiency of 5.16%, the solar cell with the nanofibre photoanode presented an efficiency of 7.28%, which is a 40% enhancement. Without question, this efficiency jump aroused by the application of nanofibres as the photoanode is attributable to the large surface area (86 m^2 g^{-1}), which favours the adsorption of a large amount of dye molecules, as well as a high scattering effect for visible light. In order to further improve the cell performance, we have to improve the open circuit voltage as well. Herein, we tried to increase the V_{oc} by depositing a blocking layer between the SnO_2:F glass and the TiO_2 photoelectrode, which will inhibit the electronic recombination at the FTO surface. The cells with the blocking layers are denoted as NF-2 and P25-2 for the nanofibre photoanode and the P25 photoanode, respectively. Moreover, the inhibited electron recombination will also increase the J_{sc}. With the compact blocking layer, the conversion cell efficiency (η) of the nanofibre cell (NF-2) significantly increased from 7.28% to 8.14% (Figure 4(a)), due to the increase in the J_{sc} from 13.69 mA cm^{-2} to 15.23 mA cm^{-2}. A similar strategy also was applied to the P25 based solar cells (P25-2), where an improvement from 5.16% to 6.03% in cell efficiency was observed. After employing the blocking layer, the cell efficiency for the nanofibre solar cell (NF-2) presented a 35% enhancement over the one with P25 photoanode (P25-2). Accordingly, the dense layer of TiO_2 in the blocking layer provides better coverage of the substrate and improves the electron transfer to the substrate. The corresponding IPCE results (quantum efficiency) are also shown in Figure 4(b). The cell made from the nanofibres showed a stronger response in the wavelengths between 400 and 700 nm compared to the one with the P25 nanopowders. No significant difference in the IPCE due to the blocking layer occurred,

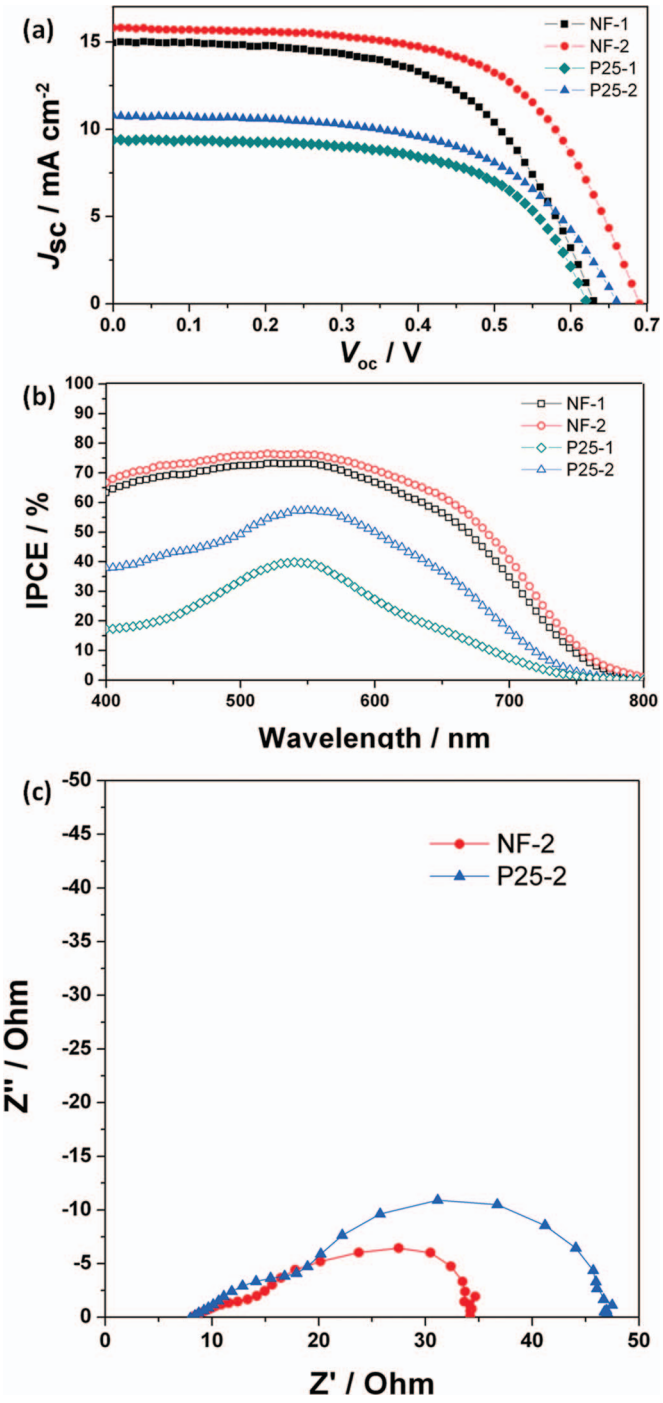

FIG. 4. (a) *J-V* curves and (b) IPCE spectra of all solar cells. (c) EIS spectra of the NF-2 and P25-2 samples.

however, between the TiO_2 nanofibre photoelectrode samples NF-1 and NF-2. Therefore, based on the application of the nanofibres as photoanode, the performance of the solar cells shows a significant enhancement, which is more than 40% superior to sample P25-1 (without the blocking layer) with the commercial Degussa P25 photoanode, due to the salient features of the 1D nanofibre structure with its large surface area (86 $m^2\ g^{-1}$) and strong light scattering effect. In order to better understand the improved electron transfer properties of the cells with the nanofibres, electrochemical impedance spectroscopy (EIS) measurements of the cells under 1 sun illumination were carried out at the V_{oc}.

The spectra are shown in Figure 4(c) for NF-2 and P25-2, both with the blocking layer. The two cells show a typical double semicircle spectrum corresponding to high frequency relaxation (which is due to the redox reaction at the charged counter electrode), as well as low frequency relaxation (which is due to the injection/recombination reactions and electron diffusion in the photoanode). Due to the low frequency characteristics of the diffusion coefficient, the electron transport time (τ_d) can be calculated using $\tau_d = 1/(2\pi f_{min})$, where f_{min} is the characteristic frequency at the minimum EIS imaginary coordinate. In the case of the nanofibre cell, the electron transport time was calculated to be 1.08 ms compared to the 1.43 ms estimated for the P25 sample. In addition, for the P25 sample, the second semicircle has a large section at ω_{min}, from $\omega_d = D/d^2$, where D is the electron diffusion coefficient and d is the film thickness. Therefore, it can be concluded that the diffusion coefficient of electrons in the P25 sample is lower than in the nanofibre sample. The electron diffusion coefficient for the P25 was calculated to be 2.97×10^{-5} $cm^2\,s^{-1}$ compared to 3.94×10^{-5} $cm^2\,s^{-1}$ for the nanofibres, which implies faster charge transport within the nanofibres.

We have successfully demonstrated that 1D TiO_2 nanofibres as electrodes provide a new alternative to the conventional electrodes (powders) in DSSCs. The 1D TiO_2 nanofibres were obtained with a high specific surface area (86 $m^2\,g^{-1}$), which led to more dye loading, more visible light scattering, and thereby, superior conversion cell efficiency (7.28%). In addition, the cells with the blocking layer as well as the mesoporous 1D TiO_2 nanofibre photoanode further increased conversion cell efficiency from 7.28% to 8.14%, which corresponds to a 35% enhancement over the cell with commercial Degussa P25 photoanodes. These novelties in 1D TiO_2 nanofibre fabrication and application will pave the way to improving TiO_2-based devices.

This work was supported by the Australian Research Council under a Discovery Project (DP1096546). We are grateful to Mr. Ali Jalili at the Intelligent Polymer Research Institute, Wollongong University for his valuable discussions.

[1] A. Fujishima, T. N. Rao, and D. A. Tryk, J. Photochem. Photobiol. C **1**, 1–21 (2000).
[2] A. Hagfeldt, G. Boschloo, L. Sun, L. Kloo, and H. Pettersson, Chem. Rev. **110**, 6595–6663 (2010).
[3] M. Grätzel, J. Photochem. Photobiol., A **164**, 3–14 (2004).
[4] J. Yan and F. Zhou, J. Mater. Chem. **21**, 9406–9418 (2011).
[5] Z.-S. Wang, H. Kawauchi, T. Kashima, and H. Arakawa, Coord. Chem. Rev. **248**, 1381–1389 (2004).
[6] K.-P. Wang and H. Teng, Appl. Phys. Lett. **91**, 173102 (2007).
[7] P.-T. Hsiao, Y.-J. Liou, and H. Teng, J. Phys. Chem. C **115**, 15018–15024 (2011).
[8] H. Yu, S. Zhang, H. Zhao, B. Xue, P. Liu, and G. Will, J. Phys. Chem. C **113**, 16277–16282 (2009).
[9] Z. Sun, J. H. Kim, T. Liao, Y. Zhao, F. Bijarbooneh, V. Malgras, and S. X. Dou, Cryst. Eng. Comm. **14**, 5472–5478 (2012).
[10] S. M. Yeon, K. D. Kyun, I. K. Jin, J. S. Mu, and K. D. Young, Nanotechnology **15**, 1861 (2004).
[11] E. Ghadiri, N. Taghavinia, S. M. Zakeeruddin, M. Grätzel, and J.-E. Moser, Nano Lett. **10**, 1632–1638 (2010).
[12] L. Yang and W. W.-F. Leung, Adv. Mater. **23**, 4559–4562 (2011).
[13] Z. Sun, J. H. Kim, Y. Zhao, F. Bijarbooneh, V. Malgras, and S. X. Dou, J. Mater. Chem. **22**, 11711–11719 (2012).
[14] B. Liu and E. S. Aydil, J. Am. Chem. Soc. **131**, 3985–3990 (2009).
[15] X.-Z. Liu, Z. Huang, K.-X. Li, H. Li, D.-M. Li, L.-Q. Chen, and Q.-B. Meng, Chin. Phys. Lett. **23**, 2606 (2006).
[16] J. N. Hart, D. Menzies, Y.-B. Cheng, G. P. Simon, and L. Spiccia, C. R. Chim. **9**, 622–626 (2006).
[17] P. Sudhagar, K. Asokan, J. H. Jung, Y.-G. Lee, S. Park, and Y. S. Kang, Nanoscale Res. Lett. **6**, 30 (2010).
[18] S. Chuangchote, T. Sagawa, and S. Yoshikawa, Appl. Phys. Lett. **93**, 033310 (2008).
[19] J. Wang and Z. Lin, Chem. Mater. **22**, 579–584 (2009).
[20] R. Mohammadpour, A. I. Zad, A. Hagfeldt, and G. Boschloo, Phys. Chem. Chem. Phys. **13**, 21487–21491 (2011).
[21] S. K. Choi, S. Kim, S. K. Lim, and H. Park, J. Phys. Chem. C **114**, 16475–16480 (2010).
[22] O. K. Varghese, M. Paulose, and C. A. Grimes, Nat. Nanotechnol. **4**, 592–597 (2009).
[23] M. Law, L. E. Greene, J. C. Johnson, R. Saykally, and P. Yang, Nature Mater. **4**, 455–459 (2005).
[24] J. B. Baxter and E. S. Aydil, Appl. Phys. Lett. **86**, 053114 (2005).
[25] S. Meng, J. Ren, and E. Kaxiras, Nano Lett. **8**, 3266–3272 (2008).
[26] B. Ding, C. Kim, H. Kim, M. Seo, and S. Park, Fibers Polym. **5**, 105–109 (2004).
[27] C. Tekmen, A. Suslu, and U. Cocen, Mater. Lett. **62**, 4470–4472 (2008).
[28] A. A. Mahdavan, S. Kalluri, D. K. Chacko, T. A. Arun, S. Nagarajan, K. R. V. Subramanian, A. S. Nair, S. V. Nair, and A. Balakrishnan, RSC Adv. **2**, 13032–13037 (2012).
[29] C.-C. Wang and J. Y. Ying, Chem. Mater. **11**, 3113–3120 (1999).
[30] Z. Sun, J. H. Kim, Y. Zhao, F. Bijarbooneh, V. Malgras, Y. Lee, Y.-M. Kang, and S. X. Dou, J. Am. Chem. Soc. **133**, 19314–19317 (2011).
[31] A. N. M. R. Ranade, H. Z. Zhang, J. F. Banfield, and S. H. Elder, Proc. Natl. Acad. Sci. U.S.A. **99**, 6476–6481 (2002).
[32] Y. Hwu, Y. D. Yao, N. F. Cheng, C. Y. Tung, and H. M. Lin, Nanostruct. Mater. **9**, 355–358 (1997).
[33] A. P. Alivisatos, Science **271**, 933–937 (1996).
[34] A. M. Smith and S. Nie, Acc. Chem. Res. **43**, 190–200 (2009).